doi:10.1016/j.jmb.2005.11.087 J. Mol. Biol. (2006) 356, 1049–1063

JMB

Available online at www.sciencedirect.com

SCIENCE DIRECT®

ELSEVIER

Molecular Dynamics Simulations and Free Energy Analyses on the Dimer Formation of an Amyloidogenic Heptapeptide from Human β2-Microglobulin: Implication for the Protofibril Structure

Hongxing Lei, Chun Wu, Zhixiang Wang and Yong Duan*

UC Davis Genome Center and Department of Applied Science One Shields Avenue, Davis CA 95616, USA

*Corresponding author

Amyloid formation is associated with many neurodegenerative diseases. Recent findings suggest that early oligomeric aggregates could be major sources of toxicity. We present a computational investigation of the first step of amyloid initiation–dimer formation of a seven residue peptide (NHVTLSQ) from human β2-microglobulin at pH 2.0, which renders +2.0 units charges to each peptide. A total of over 1.2 μs of simulations with explicit solvent and 1.0 μs of simulations with implicit solvent were conducted. Main-chain conformational restraint was applied to facilitate the formation of ordered dimers. An antiparallel β-sheet with six main-chain hydrogen bonds was dominant in the implicit solvent simulations. In contrast, no stable dimers were observed in the two negative controls, the mouse heptapeptide (KHDSMAE, +3.0 units charges) and the scrambled human heptapeptide (QVLHTSN). Explicit solvent simulations presented a more complex scenario. The wild-type human heptapeptide formed predominantly antiparallel β-sheets (~38%) although parallel ones (~12%) were also observed. Hydrophobic contacts preceded hydrogen bond saturation in the majority of the association events in the explicit solvent simulations, highlighting the important role of hydrophobic interaction in amyloid initiation. The fact that the mouse dimer dissociated immediately after the removal of conformational restraint suggests that the higher conformational entropy barrier, along with the stronger charge repulsion and weaker hydrophobic interaction, contributed to its inability to form amyloid fibril. The closeness of positive charge pairs in the dimers of the scrambled human heptapeptide may prohibit further β-sheet extension and fibril growth. Combining the results from simulations and free energy analyses, we propose that the building block for this amyloid fibril is an antiparallel dimer with a two-residue register shift and six main-chain hydrogen bonds. A double-layer protofibril structure is also proposed in which two antiparallel β-sheets face each other and are held together by hydrophobic staples and hydrogen bonds of the polar side-chains.

Keywords: amyloid protofibril filament; β2-microglobulin; molecular dynamics simulation; protein aggregation; protein folding

Introduction

Proteins carry the major functional load of biological machinery. Maintaining a normal physiological environment is critical for the proper structure and function of proteins. Under certain non-physiological conditions, proteins can partially unfold, which could lead to aggregation. Protein aggregation and occasionally ensuing amyloid fibril formation are believed to be the causes of many severe neurodegenerative diseases including Alzheimer's, Parkinson's, Huntington's, and prion diseases.[1–4] Amyloidogenesis occurs on both physiologically folded proteins and naturally unfolded proteins, and peptides with no observed

Abbreviation used: GB, generalized Born.

E-mail address of the corresponding author: duan@ucdavis.edu

sequence homology.[5] On the other hand, a remarkably similar cross β structure, with β-strands perpendicular to and hydrogen bonds parallel with the fibril axis, has been observed in the fibril structures from different sources.[6] Recent studies have attributed the toxicity to the precursors of amyloid fibrils, including misfolded proteins, soluble oligomer aggregates, globular aggregate beads, and protofibrillar structures.[7,8] Therefore, it is important to understand these early stages and the entire process of amyloid formation.

A variety of biophysical and biochemical techniques have been applied to study amyloidosis.[8,9] The techniques for detecting fibrils include Congo red binding, thioflavin T (ThT) fluorescence, transmission electron microscopy (TEM), circular dichroism (CD), and Fourier transform infrared spectroscopy (FTIR). Further structural characterization techniques include X-ray fiber diffraction, cryo-electron microscopy, and solid-state NMR (nuclear magnetic resonance) spectroscopy. By applying these techniques, it has been revealed that amyloid fibrils are generally unbranched, a few micrometers in length, and about 10 nm in diameter. Fibrils usually consist of two to six protofibrils winding around each other. One of the stabilization forces of the fibril structure is likely to be the main-chain hydrogen bonds. Apart from structural characterization of amyloid-related proteins, considerable effort has been devoted to smaller amyloid-forming peptides, mostly fragments from prion protein[10–12] and amyloid β protein.[13,14] A recent breakthrough was the high resolution structure of an amyloid-like fibril of the peptide GNNQQNY originated from yeast prion by X-ray crystallography.[15]

Despite this progress, experimental detection and characterization of early-stage species and their dynamics has been a great challenge. Detailed experimental information on the early-stage structure transformation and association has remained elusive. The need for the information on the structure and dynamics of early species, which have been linked to toxicity, has prompted many molecular simulation studies. Traditional simulations include stability studies of amyloid-prone protein monomer and dimer,[16–19] and conformation transition of short amyloid-forming peptides.[20–23] In an elegant study of this kind conducted by DeMarco and Daggett,[24] local conformational transition was observed in a prion protein. This transformed protein was then used to model protofibril and the reconstructed electron microscopy images showed decent similarity with the experimental ones. In another direction, simulations of the aggregation process at various stages have been conducted. With simplified peptide models, aggregation of relatively large systems can be studied.[25–28] Regular fibrils were observed in simulation for systems containing up to 96 peptides.[29,30] However, detailed information, including sequence-dependent features, is difficult to obtain from simplified models.

More detailed information has been revealed from aggregation simulations with all-atom models. Simulations on peptide GNNQQNY from yeast prion protein Sup35[31,32] demonstrated that the favorable parallel β-sheet conformation was stabilized by the peptide backbone dipoles and specific side-chain interactions; namely the polar side-chain "zipper" (hydrogen bonding) and the tyrosine ring stacking. It was shown in a simulation of an 11 residue peptide fragment from transthyretin (105–115)[33] that the spontaneously formed antiparallel out-of-register association was compatible with experimentally determined distances and chemical shifts. Residues 106–111 were found to be crucial for the formation of stable hydrogen bonds. In another study, a large number of short simulations (1 ns each) were conducted on five short peptides to obtain statistical information on dimer formation.[34] It was concluded that hydrophobic interaction was responsible for the initial association, as well as trapping the peptides in local minima. In order to speed the aggregation, explicit solvent was not present in the above-mentioned simulations. However, water can form explicit hydrogen bonds with peptides, which is one of the solvent properties that are not present in the existing implicit solvation models. Therefore, explicit solvent models are thought to give more complete information about the simulated aggregation process than the implicit ones.

Simulation with explicit solvent on peptide $A\beta_{16-22}$ (KLVFFAE)[35] suggested an obligatory helical intermediate in the aggregation process, while both hydrophobic and charged residues were necessary to stabilize the oligomer. Replica exchange was applied to a pentapeptide DFNKF[36] to explore the energy landscape of trimer formation, in which Asn-Asn stacking was found to act like a "glue" to greatly reduce the conformational search. Several simulations with explicit solvent have been conducted on the islet amyloid peptide NFGAIL. In a stability study of pre-constructed NFGAIL oligomers with various sizes (one to nine peptides) and different orientations,[37] oligomers with antiparallel in-sheet and parallel between-sheet organization were found to be favorable, and the stabilizing role of Phe was demonstrated by the weak stability of the negative control NAGAIL. In another study, 26 randomly oriented replicas of NFGAIL peptides aggregated into one cluster within 10 ns.[38] Preference for extended conformation and aromatic interaction was suggested to be critical for the aggregation.

We have conducted a series of simulations on peptide NFGAIL.[39–41] Hydrophobic force was shown to be the driving force to form ordered oligomers as well as disordered aggregates, which are believed to be local minima. The crucial role that Phe plays is to direct β-sheet stacking of NFGAIL to form well-ordered oligomers in which the side-chain of Phe was observed to fit right into the concave surface around Gly of the neighboring peptides. Elongation of the ordered oligomer was

dominated by a primary pathway in which peptides were first aggregated to the oligomer and slowly moved to form main-chain hydrogen bonds with one of the existing layers.

Human β2-microglobulin is one of the well-studied amyloid-forming proteins.[42–48] In the work by Ivanova *et al.*,[49] a heptapeptide fragment (NHVTLSQ) within the loop connecting the strands F and G was found to form amyloid at pH 2.0 with 2.0 M NaCl. A zipper-spine model based on this finding was proposed for the β2-microglobulin protofilament. It was also found that the corresponding heptapeptide in mouse β2-microglobulin (KHDSMAE) and a scrambled human heptapeptide (QVLHTSN) could not form amyloid fibril under the same conditions.

The human heptapeptide fragment (NHVTLSQ) is quite unique among the known amyloid-forming peptides. It does not contain aromatic residues, which are believed to act as a nucleus in many amyloid formation processes. Neither does it have continuous Asn or Gln, which can form a polar side-chain (hydrogen bond) zipper. Instead, it has a net charge of 2 (at pH 2.0) near the N terminus (NH_3^+ and His^+). We are interested in how this highly charged peptide forms amyloid without an aromatic stabilizing force and what role the charges play in the process. Following our previous works,[40,41] we applied main-chain conformational restraint in most simulations, which has been shown to greatly speed ordered peptide association. To study the role of the solvent, we conducted both explicit and continuum solvent simulations. Our focus in this work is on the very first step of amyloidogenesis-dimer formation. An amyloid protofibril model is proposed based on the simulations and free energy calculations.

Results

Dimer association in simulations with generalized Born (GB) solvation

With the main chain restrained to the β-conformation, a total of ten simulations (50 ns each) with GB solvation were conducted on the human heptapeptide (NHVTLSQ). The sampling of dimer

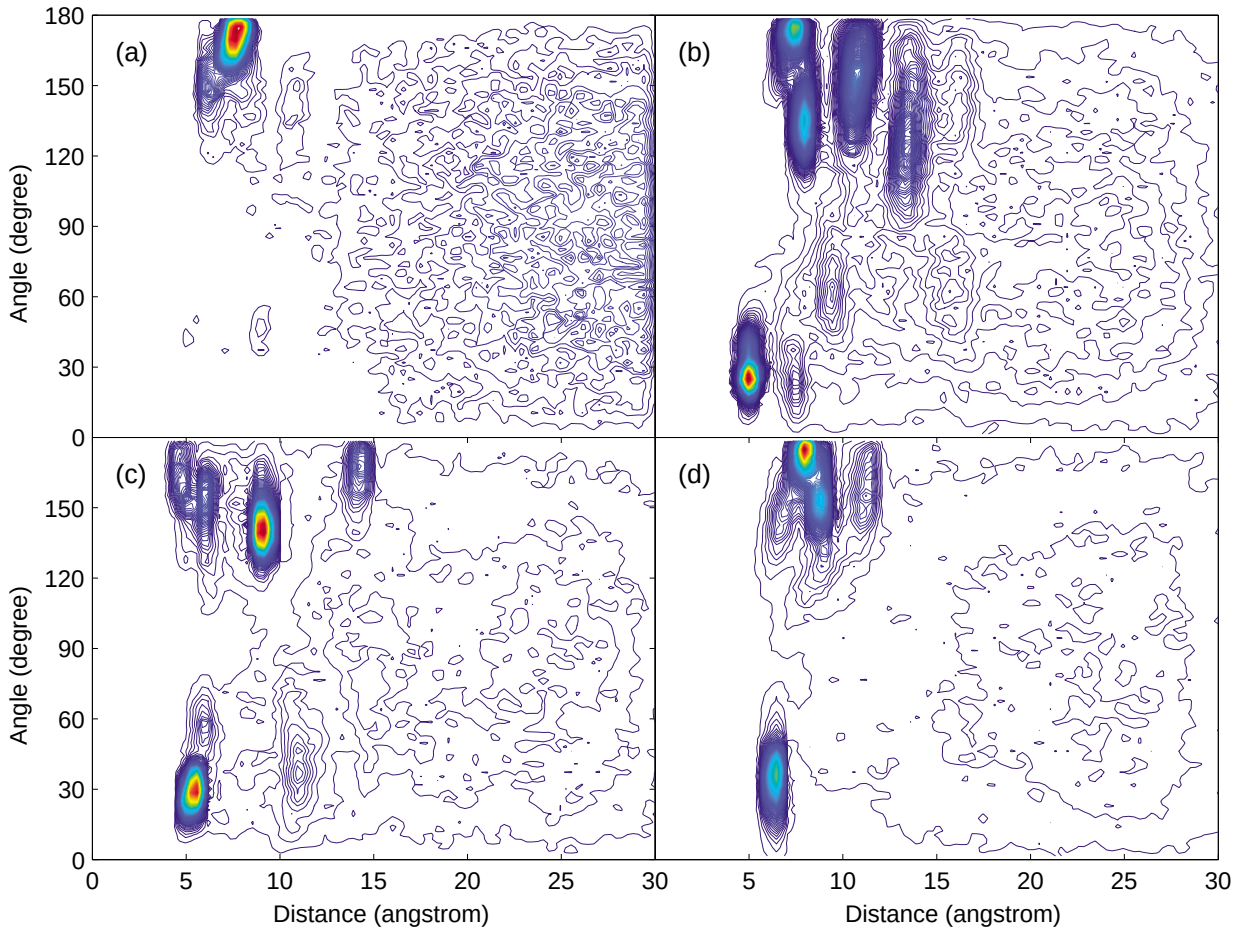

Figure 1. Sampling of dimer association states presented in two-dimensional maps based on the angle between two peptides and the distance between the C^α atoms of the central residues on each strand (with cutoff 30 Å when drawing the map). (a) The human heptapeptide in simulations with GB solvation. (b) The human heptapeptide in simulations with explicit solvent. (c) The mouse heptapeptide in simulations with explicit solvent. (d) The scrambled human heptapeptide in simulations with explicit solvent.

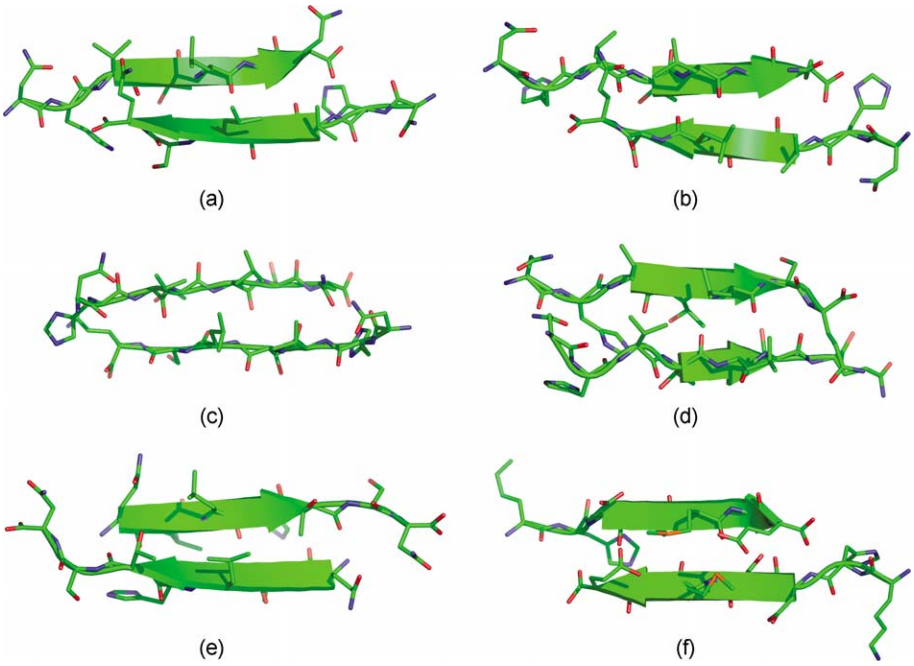

Figure 2. Highly populated β-sheets in the simulations. (a) The only dimer of the human heptapeptide in GB simulations. (b) The most populated antiparallel β-sheet of the human heptapeptide in explicit solvent simulations. (c) The second most populated antiparallel β-sheet of the human heptapeptide. (d) The most populated parallel β-sheet of the human heptapeptide in simulations with explicit solvent. (e) The most populated antiparallel β-sheet of the mouse heptapeptide in simulations with explicit solvent. (f) The most populated antiparallel β-sheet of the scrambled human heptapeptide in simulations with explicit solvent.

association is shown in Figure 1(a). The only highly populated dimer (∼14.9% of the total population) was an antiparallel β-sheet and its representative structure is shown in Figure 2(a). In this β-sheet, the two strands formed six main-chain hydrogen bonds and a ∼9° twist angle. This associated state was also stabilized by hydrophobic interactions, most prominently the inter-strand Leu–Leu interaction. The register was shifted by two residues. Presumably, the register shift and the antiparallel arrangement are due to the charge–charge repulsion of the highly charged N terminals.

In contrast, the simulations on the mouse heptapeptide (KHDSMAE) and scrambled human heptapeptide (QVLHTSN), five trajectories each and 50 ns each trajectory, did not result in any detectable well-associated dimers, suggesting that these two peptides in their monomeric forms may have much higher solubility than the human heptapeptide (NHVTLSQ). With an additional Lys residue, the mouse heptapeptide has +3 units formal positive charge near the N terminus, one more net charge than the human heptapeptide. Thus, a stronger repulsive force is expected, particularly when the peptides are in close proximity. The strength and positioning of the hydrophobic side-chains in the mouse heptapeptide may have also led to a less favorable hydrophobic interaction. As for the scrambled human heptapeptide in which the protonated His (with a +1 charge) is shifted to the central position, the repulsive force between the central charged His residues may have prevented the formation of a stable dimer. This set of simulations was consistent with the experimental observation that neither the mouse heptapeptide nor the human scrambled heptapeptide, could form amyloid under the same *in vitro* condition.

We analyzed the energetics from the simulation trajectories of the human heptapeptide and one of the results is shown in Figure 3. In Figure 3(a), the upper panel shows that the hydrophilic surface area (black line) and hydrophobic surface area (red line) dropped sharply after 18 ns. While the hydrophobic surface area reached the minimum immediately, the hydrophilic surface area continued to decline in the next 2 ns. This was consistent with the delayed main-chain hydrogen bond saturation in the middle panel compared to the Leu–Leu side-chain contact in the lower panel. However, this time delay was observed in only two trajectories. On other occasions, the saturation of a main-chain hydrogen bond occurred simultaneously with the formation of the Leu–Leu contact. Overall, both main-chain hydrogen bonding and hydrophobic side-chain interaction contributed to the dimer formation and stability.

We looked into the physical energy terms in the GB simulations. The critical energy terms of the same trajectory in Figure 3(a) are shown in Figure 3(b). Overall, the potential energy (upper panel) and van der Waals energy (middle panel) had similar features, while the combined electrostatics and GB energy (lower panel, this is solvent-screened "effective"

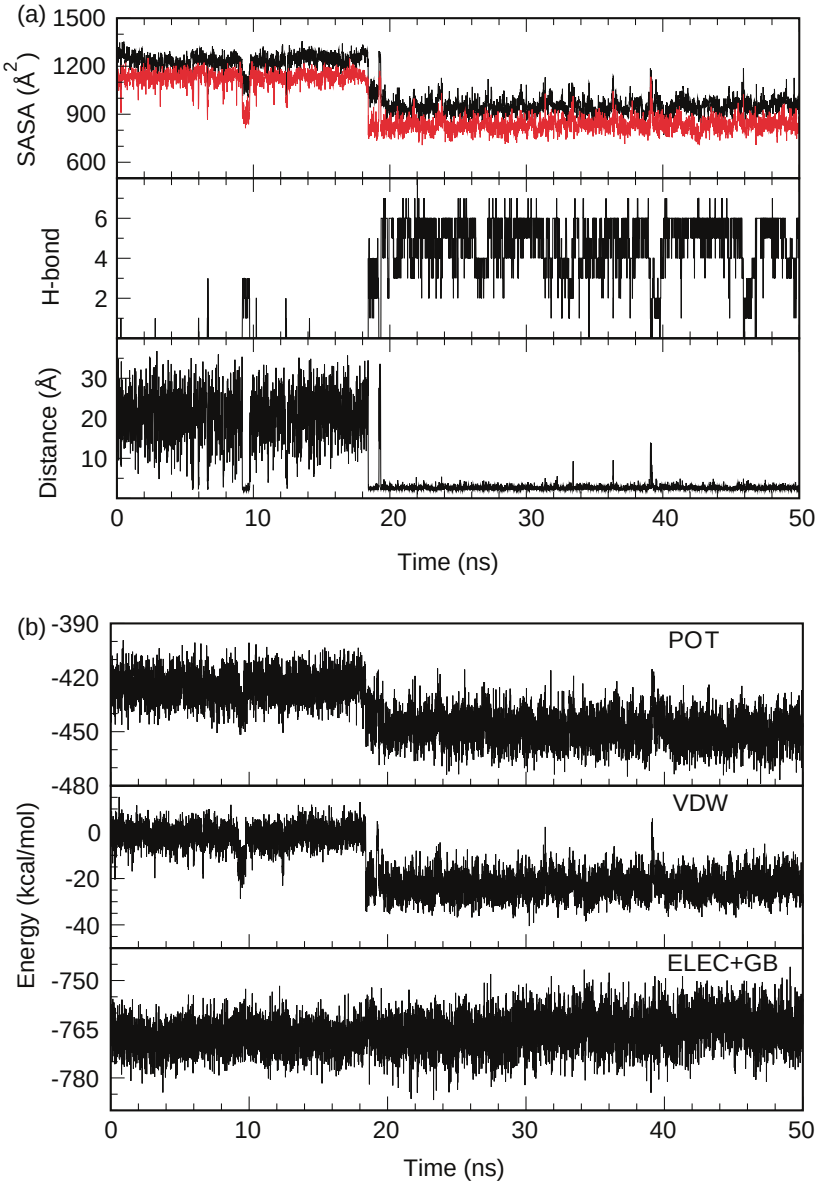

Figure 3. Time histories of various energy and structural terms in a representative GB simulation trajectory of the human heptapeptide. (a) Upper panel, hydrophilic (black) and hydrophobic (red) accessible surface area. Middle panel, main-chain hydrogen bond. Lower panel, the minimum distance between the side-chains of the Leu residues on each strand (Leu-Leu distance). (b) Upper panel, the total potential energy of the system. Middle panel, van der Waals energy. Lower panel, vacuum electrostatics plus GB energy; this is the solvent-screened effective electrostatics.

electrostatics) displayed little change other than thermal fluctuation. Figure 3(a) also demonstrates that the peptides can be partitioned into monomer and dimer states, and have consistently smaller surface areas and shorter distances in the dimer state. We therefore partitioned the trajectories into associated and unassociated regions. In this particular trajectory, according to the change of surface area, hydrogen bond, and side-chain contact, the first 18 ns was in the unassociated state and the last 30 ns was in the associated state. After association, the total potential energy decreased by ~23.9 kcal/mol. Among which, van der Waals energy decreased by ~21.2 kcal/mol and the combined electrostatics and GB energy increased by 2.4 kcal/mol (Table 1). Therefore, optimal packing of the two strands strongly favored the dimer formations. However, side-chain packing is at the expense of side-chain entropy, which is one of the major opposing forces. Since the simulations were conducted with main-chain conformational restraint, the main-chain conformational entropy should also be kept in mind as another opposing force. Dimer dissociation (and re-association) occurred in eight of the ten trajectories, implying competition among different forces and the dynamic nature of the process.

Dimer formation in simulations with explicit solvent

To understand the solvent contribution to the dimer formation further, we carried out another set of ten simulations (50 ns each) on the human heptapeptide with explicit solvent. The sampling of dimer association is shown in Figure 1(b). When compared to the GB solvation, the simulations with explicit solvent displayed a more complex scenario. Two major antiparallel association modes were sampled in the simulations (Figure 2(b),

Table 1. Energetic dissection of the populated dimer species of the human heptapeptide from the simulations with implicit and explicit solvent

		Explicit		
ΔE (kcal/mol)	Implicit antiparallel	Antiparallel 1	Antiparallel 2	Parallel
ΔE_{VDW}	−21.2	−19.4	−21.7	−27.3
ΔE_{ELE}	−42.8	−32.2	−19.9	50.5
ΔE_{INT}	−4.4	−7.3	−4.2	−1.6
ΔE_{GB}	45.2	34.1	27.5	−45.3
ΔE_{SUR}	N/A	−3.9	−4.1	−5.0
ΔE_{GBELE}	2.4	1.9	7.6	5.2
ΔE_{POT}	−23.9	−24.8	−18.3	−23.8
$\Delta E'_{POT}$	N/A	−28.7	−22.4	−28.8

ΔE_{VDW}, the change of van der Waals energy upon dimer formation. ΔE_{ELE}, the change of electrostatics energy upon dimer formation. ΔE_{INT}, the change of internal energy (bond, angle, and dihedral) upon dimer formation. ΔE_{GB}, the change of GB reaction field energy upon dimer formation. ΔE_{GBELE}, the combined change of GB and electrostatics energy upon dimer formation. ΔE_{SUR}, the change of energy due to surface area change upon dimer formation. ΔE_{POT}, the change of potential energy (excluding ΔE_{SUR}) upon dimer formation. $\Delta E'_{POT}$, the change of potential energy (including ΔE_{SUR}) upon dimer formation.

∼9.7% and (c), ∼8.4%), both had a register shift of two residues with ∼6° and ∼45° strand twist angles, respectively. Two additional antiparallel β-sheet species were observed, including one species with a three-residue register shift (11.3%) and the other with a four-residue register shift (8.4%), which will not be the focus of our further analysis. Taken together, these antiparallel species have a combined total of 37.6% snapshots. Among these antiparallel species, one of the two-residue register shift species (Figure 2(b)) was almost identical with the only dimer sampled in the GB simulation (Figure 2(a)). The other two-residue register shift species (Figure 2(c)) was also similar, albeit with much larger angle deviation from an ideal antiparallel configuration and therefore fewer main-chain hydrogen bonds.

A parallel species (Figure 2(d)) also was observed in which the His side-chains were close in space. However, the parallel species population was only 12.1%, about one-third of the antiparallel ones (which was 37.6%). Thus, in contrast to the lack of obvious preference observed in simulations of the NFGAIL peptide,[39–41] the human heptapeptide had a notably higher preference, by a factor of 3:1, towards an antiparallel β-sheet, perhaps because of the charge–charge interactions between the N terminals, which have +2 units formal charges on each peptide. It should be noted that the relative populations of different association modes changed with the number and length of the simulation trajectories. Thus, the populations reported here should be treated as only qualitative measures. Nevertheless, the observation of predominantly antiparallel β-sheets in the explicit solvent simulations, the sole formation of the same species in the GB simulations, and the lack of obvious preference in the explicit solvent simulations of NFGAIL with essentially an identical simulation protocol strongly suggest that the human heptapeptide assumes an antiparallel arrangement in the fibrils.

A representative trajectory with the formation of the ordered antiparallel β-sheet conformation is shown in Figure 4(a). There was an "intermediate" dimer (between 2 ns and 20 ns) prior to the formation of the ordered dimer. Interestingly, this intermediate dimer formed in the absence of the hydrophobic Leu–Leu interaction as shown in the lower panel (structure not shown). During the formation of the ordered dimer, the hydrophobic Leu–Leu contact formed near 21 ns, whereas the saturation of the main-chain hydrogen bond occurred near 24 ns. Another trajectory that led to the formation of the twisted antiparallel conformation is shown in Figure 4(b). The hydrophobic and hydrophilic surface areas decreased simultaneously near 8 ns (upper panel). However, this was initiated by the hydrophobic Leu–Leu contact (lower panel) rather than main-chain hydrogen bonding (middle panel), which had a 500 ps delay. In fact, the delay of hydrogen bond saturation (compared to the formation of hydrophobic contact) was observed in most of the dimer association events in the simulations of the human heptapeptide with explicit solvent.

We further analyzed the three populated dimers (two antiparallel β-sheet and one parallel β-sheet) found from the simulations with explicit solvent using the MM-GB/SA method[50] and the results are shown in Table 1. The analysis suggests that the antiparallel and parallel β-sheets are stabilized by different forces. For the two antiparallel dimers, electrostatics decreased by 32.2 kcal/mol and 19.9 kcal/mol, respectively, upon formation. In contrast, due to charge repulsion, electrostatics increased 50.5 kcal/mol upon formation of the parallel dimer. The change in GB reaction field energy compensated for most of the changes in electrostatics, leaving a net increase of only 1.9 kcal/mol and 7.6 kcal/mol for the antiparallel dimers and 5.2 kcal/mol for the parallel dimer. On the other hand, the parallel β-sheet gained more favorable van der Waals energy (−27.3 kcal/mol) than the antiparallel ones (−19.4 kcal/mol and −21.7 kcal/mol). Internal energy slightly favored the antiparallel dimers (−7.3 kcal/mol and −4.2 kcal/mol) over the parallel dimer (−1.6 kcal/mol). The slight gain in favorable

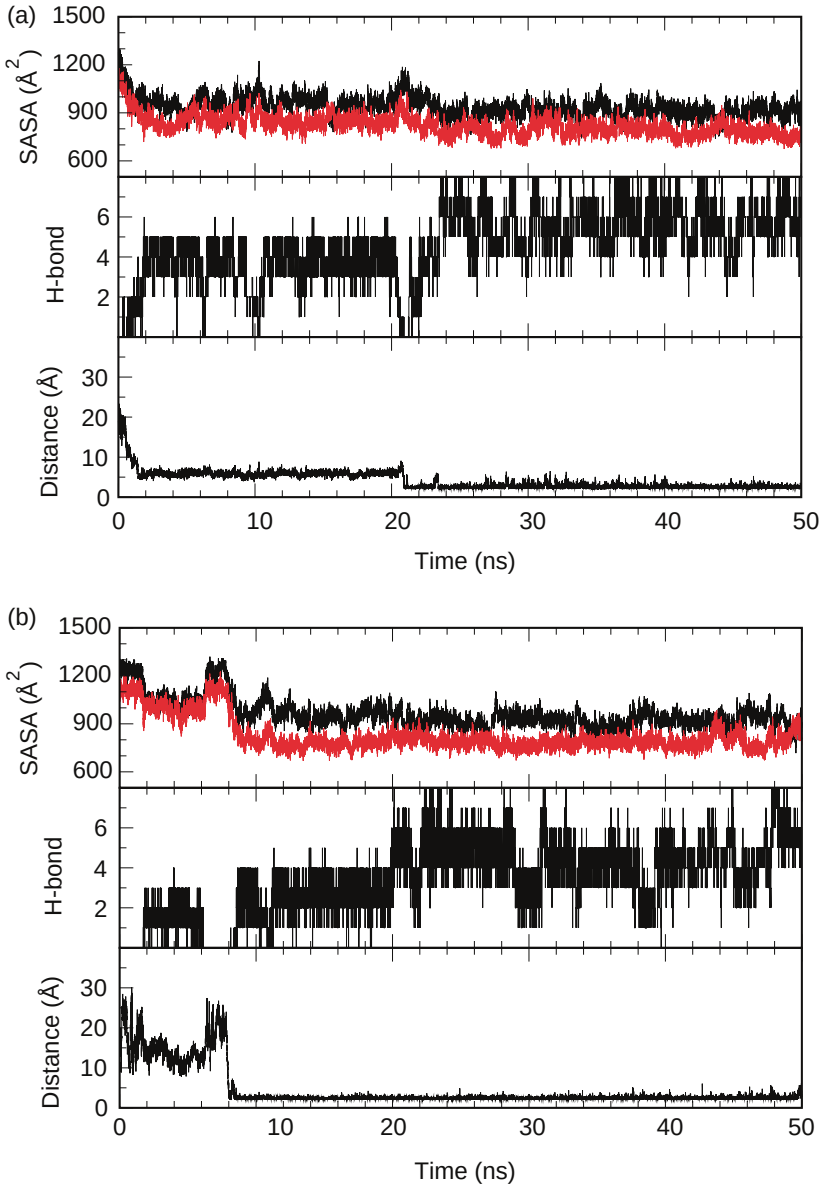

Figure 4. Time histories of various energy terms in two representative simulations with explicit solvent of the human heptapeptide. (a) A trajectory led to the most populated antiparallel mode. (b) A trajectory led to the second most populated antiparallel mode. For details please refer to the legend to Figure 3.

energy due to surface area change was similar for all three conformations. Overall, the total potential energy decreases of the parallel β-sheet (−28.8 kcal/mol) and the regular antiparallel β-sheet (−28.7 kcal/mol) were notably more than that of the twisted antiparallel β-sheet (−22.4 kcal/mol).

We also compared the energy components of the two similar antiparallel β-sheets from the simulations with implicit and explicit solvent. The potential energy changes (excluding the surface area term, since it was disabled in the GB simulation) were −23.9 kcal/mol for the β-sheet from simulation with implicit solvent and −24.8 kcal/mol for the simulation with explicit solvent. The difference in the electrostatics was compensated by the difference in GB reaction field energy, leading to a similar change in "effective" electrostatics, (2.4 kcal/mol for implicit and 1.9 kcal/mol for explicit). The van der Waals energy slightly favored the one from simulations with implicit solvent (−21.2 kcal/mol *versus* −19.4 kcal/mol), while the internal energy slightly favored the one from simulations with explicit solvent (−7.3 kcal/mol *versus* −4.4 kcal/mol).

Simulation of the controls with explicit solvent

Five simulations (50 ns each) were conducted for each of the two negative control peptides: the mouse heptapeptide and the scrambled human heptapeptide. With the main-chain restrained in β-conformation, dimer association events were also observed. The sampling of dimer association is shown in Figure 1(c) and (d) for the mouse heptapeptide and the scrambled human heptapeptide, respectively. Representative structures are displayed in Figure 2(e) and (f). The mouse dimer was primarily antiparallel with a two-residue register shift, stabilized by six main-chain hydrogen

bonds and a hydrophobic Met–Met inter-strand interaction. The scrambled human dimer was also primarily antiparallel with a two-residue register shift, stabilized by six main-chain hydrogen bonds and hydrophobic Leu–Leu and Val–Val interactions, one on each face of the β-sheet.

These results from simulations with explicit solvent were complementary to what we observed in the GB simulations in which only the wild-type human heptapeptide formed a stable β-sheet. We examined the effect of main-chain conformational restraint by removal of conformational restraints of three representative antiparallel dimers, one from each of the heptapeptide. The mouse dimer dissociated within 1 ns, while the other two dimers were much more stable (the human dimer was stable up to 7 ns, and the scrambled human dimer was stable throughout the 10 ns simulation). Therefore, the large entropy loss upon dimer formation may be an important factor that keeps the mouse heptapeptide from forming a stable dimer and the amyloid initiation would have to overcome this additional barrier. As for the scrambled human heptapeptide, we found a pair of unfavorable His^+ to NH_3^+ interactions at both ends of the dimer. There are two tentative interpretations for the inability of the scrambled human heptapeptide to form amyloid. First, it could be that the observed dimer is marginally stable, while further extension of this β-sheet is prohibited because of the strong charge–charge repulsion. Second, it is possible that the strength of the above-mentioned charge–charge interaction is underappreciated in the explicit force field used in this study. With stronger charge–charge repulsion, the observed scrambled human dimer may not populate (as we observed in the GB simulations).

Conformational preference of monomers

The residue identity has a major impact on the conformational preference of peptides. According to a statistical index,[51] the human heptapeptide has a similar preference for helix (average 1.03) and sheet (average 1.04), while the mouse heptapeptide has a much stronger preference for helix (average 1.22) over sheet (average 0.88). These are consistent with the observations made in simulations on the three monomers shown in Table 2. In these simulations, both human heptapeptide and its scrambled version exhibited notably higher population (average 29% to 36%) than the mouse heptapeptide (19%) in the β-extended conformation. Furthermore, both the identity of the amino acid and the local environment can affect the configuration of each residue. For example, the populations of His^2 were almost identical in the human and mouse heptapeptides, while His^4 in the scrambled human heptapeptide shifted from PPII to β conformations. The ability to form stable or transient hydrogen bonds by the side-chains of polar residues (Asn, Gln, Ser, Thr, etc.) can also have a major impact on the conformation of the peptide.

Table 2. Populations of the conformational states of all non-terminal residues in the monomer simulations with explicit solvent

		Conformational state			
		Beta	PPII	Alpha	Others
Human	His2	27.8	72.0	0.1	0.1
7-mer	Val3	68.2	31.6	0.0	0.2
	Thr4	16.5	16.6	66.6	0.4
	Leu5	20.8	14.4	64.2	0.6
	Ser6	11.6	6.9	81.1	0.5
	Average	29.0	28.3	42.4	0.4
Scrambled	Val2	58.5	41.4	0.0	0.1
human	Leu3	21.5	26.7	51.5	0.3
7-mer	His4	42.2	56.9	0.7	0.2
	Thr5	36.5	47.2	15.7	0.6
	Ser6	20.5	16.0	63.0	0.5
	Average	35.8	37.6	26.2	0.3
Mouse	His2	28.3	71.3	0.2	0.2
7-mer	Asp3	41.7	56.8	0.5	1.0
	Ser4	7.9	3.5	88.3	0.3
	Met5	5.6	4.1	90.3	0.1
	Ala6	13.2	11.2	73.7	1.9
	Average	19.3	29.4	50.6	0.7

When compared to the human heptapeptide, the mouse heptapeptide had a lower population in β-extended conformation and a higher population in α-helical state, consistent with the measure based on average secondary structure propensity. This partly explains why the human heptapeptide could form regular amyloid while the mouse heptapeptide could only form amorphous aggregates.

We further examined the most populated peptide conformations by clustering. The three highest populated conformations for each of the three peptides are shown in Figure 5. As we may expect, coiled structures were predominant in all monomer simulations. The structural feature was similar for both the human heptapeptide (upper panel) and the mouse heptapeptide (lower panel). Consistent with the data in Table 2, the N-terminal residues were in a more extended conformation and the C-terminal residues were more coiled. The most populated clusters of the two peptides were similar in conformation but different in population, showing lower propensity for the mouse heptapeptide in the extended conformation.

Dimer association without conformational restraint

We embraced the technique of conformational restraint to facilitate the formation of ordered β-dimer and β-sheets in manageable simulation time, allowing us to look for candidates that could extend to form amyloid protofibrils. This also allows us to examine the stabilizing forces that help to initiate the amyloid formation. However, simulations with conformational restraints could not provide information on conformational transitions. Therefore, we conducted a 50 ns explicit solvent simulation on the human heptapeptide dimer without conformational restraint. Consistent

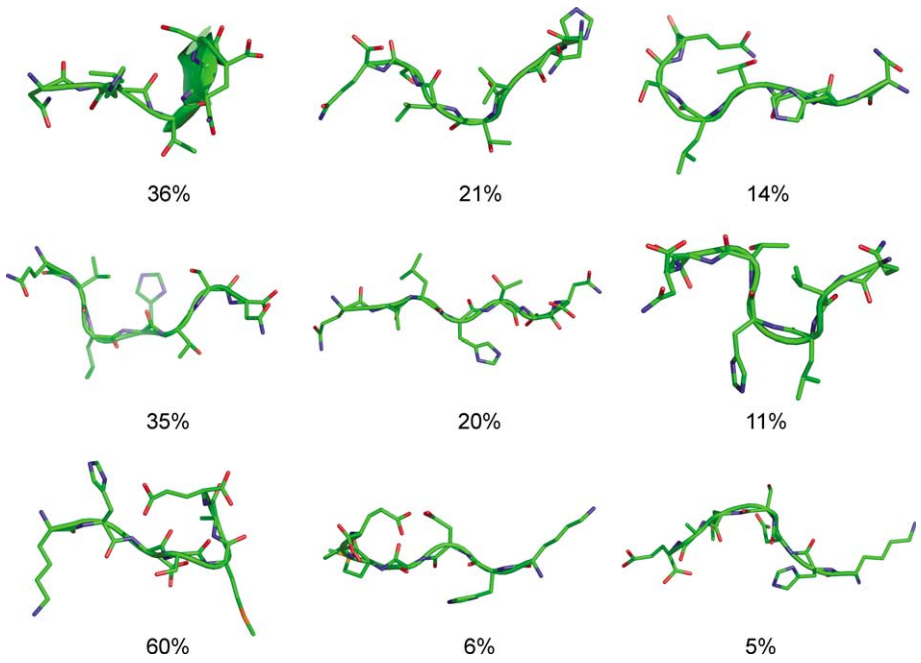

Figure 5. Representative conformations (with population indicated) in the monomer simulations with explicit solvent. Upper panel, the human heptapeptide. Middle panel, the scrambled human heptapeptide. Lower panel, the mouse heptapeptide.

with the monomer simulation, the individual strands were not in an ideal β-conformation.

Due to the slow diffusion of the peptides and the marginal stability of the dimers, the peptides were separated during most of the 50 ns simulation. In order to form an ordered dimer, the encountered peptides need to be in a relatively extended conformation and form specific and stable contacts. Prior to that, a great number of local minima on the energy surface may be sampled. Because the rate of association is controlled by diffusion, diffusion would play an important role in the dimer formation. Nevertheless, because the likelihood of the existence of two extended monomers in the nearby vicinity would be much greater in a system with a large number of peptides, an ordered dimer could be significantly easier to form in solutions, which could become the initial nucleus of amyloid fibrils.

A few transient dimer associations were observed during the 50 ns simulation (Figures 6 and 7). The associations were stabilized mainly by hydrophobic contacts, which again highlights the important roles that hydrophobic force plays in the early stage of aggregation. The peptides were found in the extended forms in some of the dimers

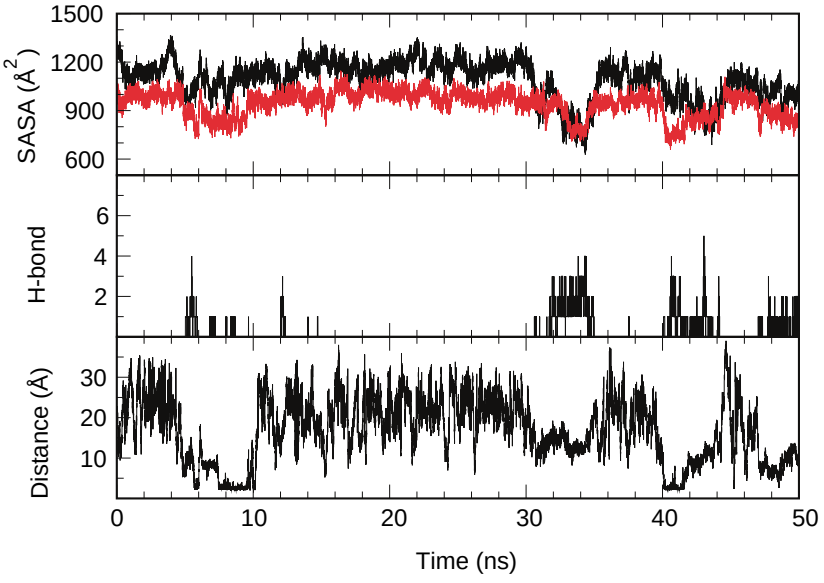

Figure 6. Time histories of various driving forces in the simulation with explicit solvent without conformational restraint for the human heptapeptide. For details please refer to the legend to Figure 3.

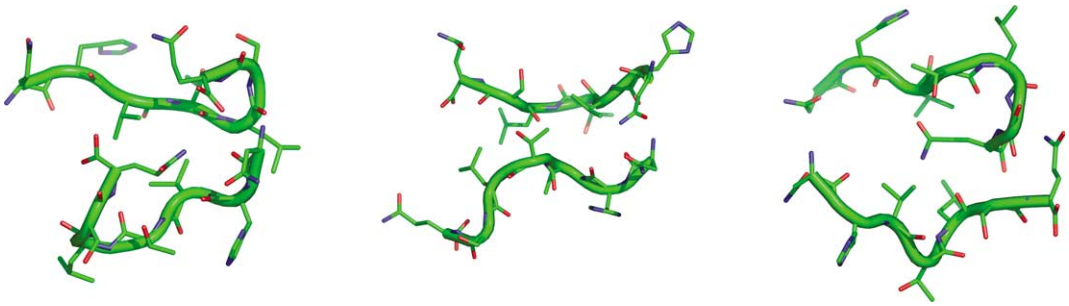

Figure 7. Representative dimer structures in the simulation with explicit solvent without conformational restraint for the human heptapeptide.

(Figures 6 and 7). Both parallel and antiparallel associations were observed. A few cross-strand main-chain hydrogen bonds also formed in the associated states. However, these hydrogen bonds appeared to be insufficient to stabilize the dimers to the β-sheet conformation and the dimers dissipated quickly. This was in sharp contrast to the stable β-sheets formed in the constrained simulations. It is clear that dimer stability is intimately coupled to peptide conformation and conformational entropy. We should also note, however, that the ultra-fast association rate in the simulations with restraint (∼20 ns) was highly exaggerated due to the assumption that two extended monomers are always close in space and do not change conformation during the diffusion process. Apparently, peptide conformation and conformational transition can have a major impact to both association modes and dimer (oligomer) stability.

Discussion

Energetics and force field development

Quantitative energetic analysis has been a challenge for simulations as well as experimental studies of peptide association. Formation of a peptide dimer is the result of the interplay between enthalpy and entropy. Upon dimer formation, both enthalpy and the conformational entropy of the peptides decrease, while the former is favorable and the latter is unfavorable. The components of the enthalpy include favorable van der Waals, electrostatics (especially hydrogen bond), unfavorable charge repulsion, and others. Solvent also plays important roles in this process by driving the hydrophobic groups towards each other, by preferentially solvating the polar groups and by forming transient hydrogen bonds with peptides, among many other effects. The most difficult part of energetic analysis lies in the solvent contribution, because of the massive rearrangement of solvent hydrogen-bonding network and the more intriguing solvent entropy change. Ions add another dimension of complexity to this problem, since ions can interact with solvent molecules, peptides and with each other. Problems can also originate from the enormous gap between the time for amyloid formation (days) and the time accessible in simulations (currently microseconds or less).

We present in Table 1 the potential energy changes upon formation of the three primary β-sheet species. The entropy of the peptides consists of both backbone and side-chain conformational entropy. The antiparallel β-sheets had a two-residue register shift, therefore ten of the 14 residues were restricted in the β-state. The parallel β-sheet did not have a register shift, therefore all 14 residues were restricted in the β-state. The entropy loss by restricting the backbone in the extended state is estimated to be ∼4.8 cal/(mol K residue).[52] So the backbone entropy loss (we use $T\Delta S$ with standard $T=300$ K) is ∼14.3 kcal/mol for the antiparallel β-sheets and ∼20.0 kcal/mol for the parallel β-sheet. According to a mean side- chain entropy scale,[53] the side-chain entropy loss is ∼8.4 kcal/mol for the antiparallel β-sheets and ∼12.3 kcal/mol for the parallel β-sheet. The total loss of conformational entropy is ∼22.7 kcal/mol for the antiparallel β-sheets and ∼32.3 kcal/mol for the parallel β-sheet. When combining the potential energy change with the entropy change, the free energy of dimerization is −5.0 kcal/mol and +0.3 kcal/mol for the two antiparallel β-sheets, and +4.5 kcal/mol for the parallel β-sheet. This could rationalize why the ordered antiparallel β-sheet was the sole populated dimer observed in the GB simulations.

We recognize that there are substantial errors in the free energy estimation. There are also various approaches to evaluate each of the three energy components (potential energy, backbone entropy, and side-chain entropy). Direct calculation of absolute free energy in explicit solvent is still an unsolved task at the moment and is beyond the scope of this work. These are sources of uncertainty. Nevertheless, this free energy estimation can still give us qualitative information on the relative stability of the dimer conformations in implicit solvent.

Simulation force fields are under continuous development. Notable secondary structure bias was observed in early AMBER force fields (bias to α-helix in ff94 and bias to β-extended in ff96). The latest force field ff03 developed by our group has

been shown to provide a better balance.[54] However, non-physical assumptions in the point-charge framework will likely lead to certain artifacts that increase the difficulty in interpreting simulation results. In our current study, the simulation results with GB solvation were more consistent with the experimental data. This by no means suggests that the GB solvation model is superior to explicit solvent. It is likely that (different) problems exist in both models. For example, charge interaction could have been overestimated in the GB solvation model due to the underestimation of solvent and ion screening effects. On the other hand, limited sampling in simulations with explicit solvent makes the equilibrium property less certain. Generally speaking, implicit solvation models are less accurate than explicit solvation models. However, kinetic trap is a more serious problem in simulations with explicit solvent than those with implicit solvent. Therefore, combining the results from both types of simulations and identifying the consistent feature may give a better understanding of the simulated system. The addition of ions in simulation can also be problematic. In a few trials with 2 M NaCl (experimental condition), ion crystals were formed in the simulations. This is why we chose 0.2 M NaCl in our simulations. We are looking into all these problems and will take them into account in future development.

Prediction of amyloid protofibril structure

The simulations clearly showed that the human heptapeptide prefers an antiparallel β-sheet arrangement. In the simulations with the GB continuum model, a stable antiparallel β-sheet was the only dominant species observed in the simulations. In the simulations with the explicit solvent TIP3P model, four antiparallel β-sheet species were observed with a combined population of 37.6% of all snapshots. Although a parallel β-sheet was also observed, its population was only 12.1%, notably lower than the antiparallel β-sheets. Among the antiparallel β-sheets observed in the simulations, a two-residue register shift species was observed in simulations with both GB and explicit solvent. Free energy analyses also indicated that this particular species was the most favorable state. Therefore, we propose this antiparallel β-sheet with six main-chain hydrogen bonds and a two-residue register shift as the building block for the fibril formed by the human heptapeptide. Furthermore, based on this β-sheet structure, we constructed a putative model for a layer of amyloid fiber. In this model, the peptides are in an antiparallel β-sheet conformation with a two-residue register shift (Figure 8(a)).

One interesting feature of this conformation is that the N-terminal groups and the protonated His side-chains, both have a +1.0 unit formal charge, protrude from the main body of the β-sheet and are exposed to solvent. Also interesting is the partition of hydrophobic and polar surfaces. As shown in Figure 8(a), Val and Leu are on one side of the β-sheet and Thr and Ser are on the other side. The hydrophobic surface appears to be a nice template to dock another complementary hydrophobic surface. Indeed, it makes energetic sense to have the two hydrophobic faces in contact, forming a two-layer fibril building block with the hydrophobic faces sandwiched inside and the two hydrophilic faces exposed to solvent.

We thus constructed a double-layer protofibril filament by placing two eight-strand β-sheets together with the hydrophobic surfaces facing each other. The filament was then subjected to energy minimization. The 16-mer double-layer β-sheet is shown in Figure 8(b). In this construct, the inner core comprises the Val and Leu side-chains, forming hydrophobic staples. The two hydrophilic side-chains, Asn and Gln, also form cross-layer hydrogen bonds, further stabilizing the double layer structure. The polar side-chains are exposed to solvent and the charged groups are outside the main body of the fibril and are fully solvated. The filament is slightly twisted along the hydrogen bond direction, by about 14° per step.

Conclusions

Amyloid fibrils have similar morphology, yet the peptides that are capable of forming amyloid are very diverse. Generally speaking, hydrophobicity, hydrophobic pattern, net charge, and conformational preference of the peptide all have a major impact on the aggregation propensity. Furthermore, the pathways to fibrilization may be as diverse as the peptides themselves. It has been pointed out in some simulation studies that aromatic ring stacking and "polar zipper" (continuous Gln or Asn) are vital in the early aggregation of some peptides. Here, we investigate the mechanism of amyloid formation by a seven-residue peptide from human β2-microglobulin. We are particularly interested in this peptide because it has net charge (+2) and does not have either aromatic residues or continuous Gln (or Asn) as in other known amyloid-forming peptides.

In the majority of our simulations we applied a main-chain conformational restraint to facilitate dimer association. In most simulations with explicit solvent, a lag phase was observed between the initiation of hydrophobic contact and saturation of hydrogen bonding. We propose that hydrophobic interaction is the driving force for the dimer formation of the human heptapeptide, while main-chain hydrogen bonds provide subsequent stabilization. In the GB simulations, the antiparallel β-sheet was the only major associated mode for the human heptapeptide, whereas there was no dimer formation in the other two negative control peptides. In the simulations with explicit solvent, multiple association modes were populated for all three heptapeptides with predominantly antiparallel β-sheets in the human heptapeptide. Simulations on the representative dimers in

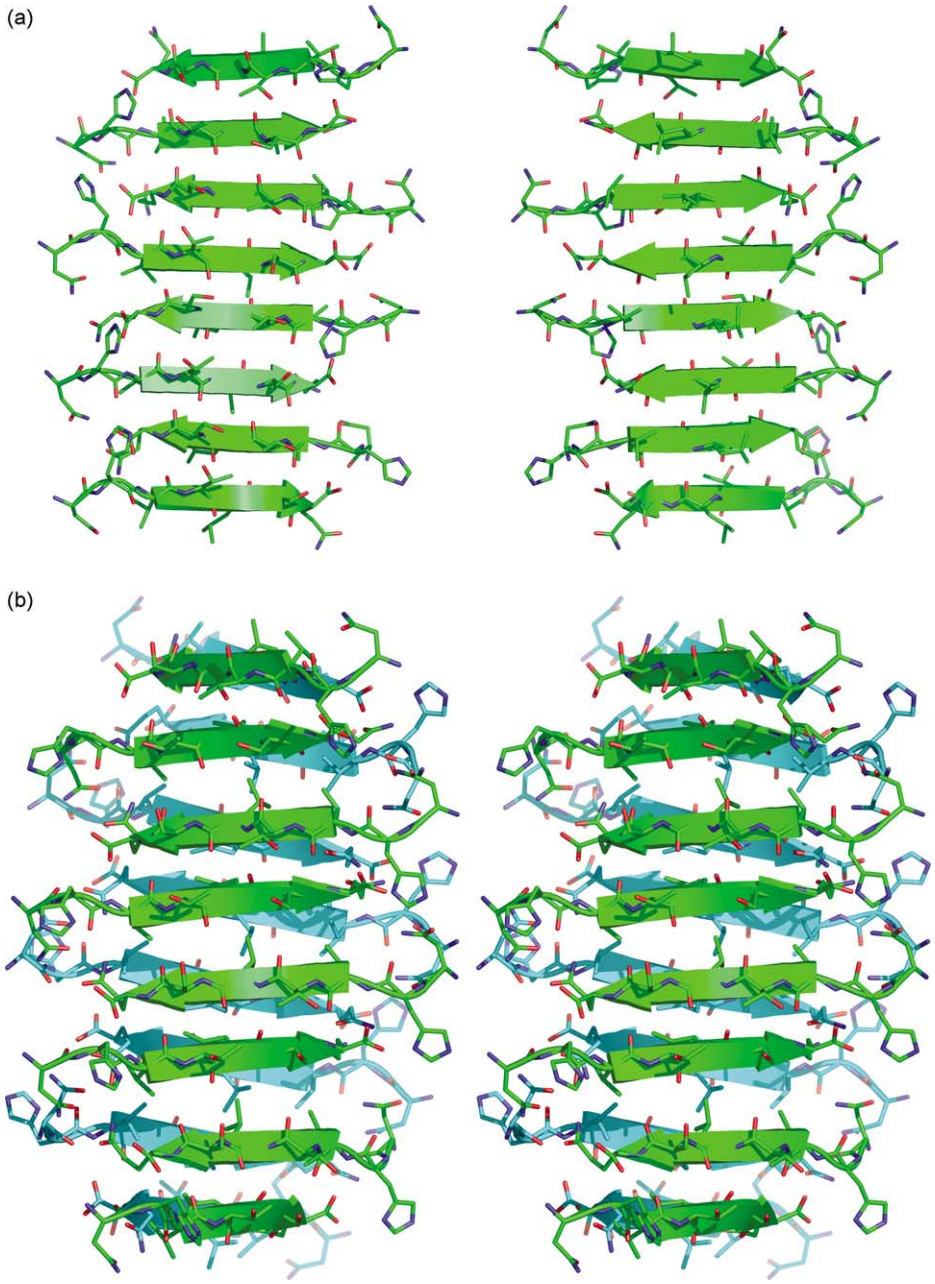

Figure 8. Proposed models of the amyloid protofibril formed by the human heptapeptide. (a) A single-layer β-sheet structure, showing hydrophilic (left) and hydrophobic sides (right) of the sheet. (b) A stereo view of the relaxed double-layer amyloid protofibril filament with hydrophobic surfaces inside.

the absence of the conformational restraint resulted in the immediate dissociation of the mouse dimer, suggesting that the conformational entropy barrier was an important factor preventing the mouse heptapeptide from forming (stable) amyloid. As for the scrambled human heptapeptide, the closeness of positive charge pairs in the dimer may be the main factor preventing further extension of the β-sheet and fibril formation.

We investigated the conformational preference of the three heptapeptides using free monomer simulations with explicit solvent. The mouse dimer displayed the highest propensity to form a coiled structure, consistent with the lowest stability of the mouse dimer. The similar features displayed in the monomer simulations of the wild-type and scrambled human heptapeptides suggest that factors other than conformational preference are also critical in amyloid formation. More specifically, the positioning of the charged and hydrophobic residues will likely affect the aggregation propensity. In the simulation of two human heptapeptides without conformational restraint, dimer formation was also observed in an apparently diffusion-controlled process coupled with conformational sampling. The peptides were found in the extended forms in some of the dimers and were aligned either antiparallel or parallel. However, there was only sporadic formation

of main-chain hydrogen bonds. Taken together, this set of simulations suggests that conformational preference of the peptide is critical for the kinetic association rate, provided that a thermodynamically stable association exists.

Free energy analyses suggest that the same antiparallel β-sheet found in the simulations with both implicit and explicit solvent is the most stable conformation. We thus propose this β-sheet as the basic building block for the protofibril. A multi-strand β-sheet was constructed that revealed a clear partition of hydrophobic and hydrophilic surfaces. A double-layer protofibril filament was made by docking two single-layer β-sheets by placing the hydrophobic faces of two β-sheets against each other. This filament may be stabilized by the hydrophobic core formed by the Val and Leu side-chains sandwiched by the β-sheet main chains. Hydrogen bond interaction of the polar side-chains (Asn and Gln) may also increase the stability.

Methods

All the simulations were conducted with the AMBER simulation package.† The all-atom point-charge force field ff03 was chosen to represent the peptides.[54] We conducted simulations with both implicit and explicit solvent. In the simulations with implicit solvent, the generalized Born (GB) approach was chosen to mimic the solvation effect.[55] To maintain β-conformation, the main-chain Φ and Ψ torsion angles were restrained at $-129(\pm 30)°$, and $124(\pm 30)°$, respectively, to maintain the β-extended conformation by a flat-well restraining function with a force constant of 20.0 kcal mol^{-1} $radius^{-2}$ when deviation from the ideal values exceeds $\pm 30°$. In order to prevent the peptides from flying away from one another, the distance between the central residues of the two strands was restrained to within 30 Å by a flat-well restraining function (i.e. there was no restraining force when the two strands were closer than 30 Å) with a force constant of 20.0 $kcal^{-1}$ mol^{-1} $Å^{-2}$. This distance restraint was only applied to GB simulations. The residues His, Asp, and Glu, and the C-terminal COO– group were protonated to mimic the acidic experimental condition at pH 2.0.[49] The temperature was set to 310 K. The ionic strength was set to 0.2 M. The cutoff for both general non-bonded interaction and GB pairwise summation were set to 12 Å. The time-step was 1 fs in all the GB simulations.

Water solvent was represented by the TIP3P model in the simulations with explicit solvent. Peptides were immersed in a water box of a truncated octahedron with a minimum distance of 9–10 Å between the peptide and the box surface. When two peptides were put into the same box, they were 20 Å apart and parallel with each other. Na^+ and Cl^- were added to the box to neutralize the system and to mimic the ionic strength at ~0.2 M salt concentration (NaCl). The sizes of the system were approximately 8000 atoms. The simulation temperature was set at 310 K to mimic the experimental condition. The time-step was 2 fs in all simulations with explicit solvent. After the initial minimization (500 steps steepest descent plus 500 steps conjugate gradient), the systems were equilibrated for 20 ps with a position restraint imposed on peptide atoms. The systems were heated from 100 K to 310 K while the target pressure was maintained at 1 atm. This was followed by a 30 ps constant volume relaxation with a main-chain dihedral restraint on peptides. Five or ten 50 ns production runs (ten for the human heptapeptide and five for the two controls) were then followed, starting from the same conformation with a different random velocity assignment. The same main-chain conformational restraint was applied. The cutoff for van der Waals interaction was set to 9 Å. A particle mesh Ewald (PME) method was used for long-range electrostatic treatment.[56] SHAKE was applied for bond constraints. Slow-varying terms were evaluated every two steps.[57] System coordinates were saved every 2 ps.

Clustering was conducted on each individual trajectory. The criterion for cluster was pairwise RMSD (root-mean-square deviation) below 2.0 Å between each member and the center of the cluster. The ten most populated clusters in each trajectory were selected for further examination. The distance between the C^α atoms of the central residues on each strand was calculated to evaluate the closeness of the two strands. The angle between the two strands, omitting terminal residues, was calculated to determine whether the association was in parallel or antiparallel mode. The populations of the dimer species were based on the sampling map (Figure 1) using a boundary distance and angle as cutoff. To monitor hydrophobic contact, the minimum distances between each pair of hydrophobic side-chains were calculated. Solvent-accessible surface areas (SASA) were determined using the method of Lee and Richards with 1.4 Å probe radius.[58] The radii of peptide atoms were taken from the AMBER force field. Atoms N and O were defined as polar, atoms S and C were defined as apolar (except for carbonyl carbon atoms). A simple criterion for a hydrogen bond was adopted, the cutoff for donor–acceptor distance was set to 3.5 Å, and no angular restrictions were applied.

In the monomer simulations, the main-chain dihedrals Φ and ψ of each non-terminal residue were calculated for each snapshot saved. Conformational states were defined by Φ and ψ torsion angles. The alpha state is the conformation with $-180° < \Phi < -10°$ and $-100° < \psi < 50°$. The beta state is the conformation with $-180° < \Phi < -90°$ and $50° < \psi < 180°$. The PPII state is the conformation with $-90° < \Phi < -10°$ and in $50° < \psi < 180°$. The beta and PPII states also include corresponding regions with Φ and/or ψ changed between 180° and −180°.

Energy evaluation was conducted on four dimer species of the human heptapeptide, one from the simulations with implicit solvent and three from the simulations with explicit solvent. Energy of the unassociated state was also evaluated as a reference. Dimer and unassociated species were selected based on surface area, main-chain hydrogen bond, and side-chain contact. For the simulations with implicit solvent, energy terms were directly extracted from the output file. For the simulations with explicit solvent, energy terms were evaluated using the GBSA module in the AMBER package, and the same unassociated reference was used for all three dimer species (two antiparallel dimers and one parallel dimer). We also compared using the unassociated states from the restrained and unrestrained simulations as a reference state and no significant difference was found.

† http://amber.scripps.edu

Acknowledgements

This work was supported by research grants from NIH (grant nos GM64458 and GM67168 to Y.D.). We

thank an anonymous reviewer for helpful comments. Usage of Pymol, VMD, and Rasmol graphics packages is gratefully acknowledged.

References

1. Rochet, J. C. & Lansbury, P. T. (2000). Amyloid fibrillogenesis: themes and variations. *Curr. Opin. Struct. Biol.* **10**, 60–68.
2. Dobson, C. M. (2004). Protein chemistry. In the footsteps of alchemists. *Science*, **304**, 1259–1262.
3. Ross, C. A. & Poirier, M. A. (2004). Protein aggregation and neurodegenerative disease. *Nature Med.* **10**, S10–S17.
4. Bossy-Wetzel, E., Schwarzenbacher, R. & Lipton, S. A. (2004). Molecular pathways to neurodegeneration. *Nature Med.* **10**, S2–S9.
5. Uversky, V. N. & Fink, A. L. (2004). Conformational constraints for amyloid fibrillation: the importance of being unfolded. *Biochim. Biophys. Acta*, **1698**, 131–153.
6. Stefani, M. (2004). Protein misfolding and aggregation: new examples in medicine and biology of the dark side of the protein world. *Biochim. Biophys. Acta*, **1739**, 5–25.
7. Caughey, B. & Lansbury, P. T. (2003). Protofibrils, pores, fibrils, and neurodegeneration: separating the responsible protein aggregates from the innocent bystanders. *Annu. Rev. Neuro.* **26**, 267–298.
8. Nilsson, M. R. (2004). Techniques to study amyloid fibril formation *in vitro*. *Methods*, **34**, 151–160.
9. Dobson, C. M. (2004). Experimental investigation of protein folding and misfolding. *Methods*, **34**, 4–14.
10. Satheeshkumar, K. S. & Jayakumar, R. (2003). Conformational polymorphism of the amyloidogenic peptide homologous to residues 113–127 of the prion protein. *Biophys. J.* **85**, 473–483.
11. Megy, S., Bertho, G., Kozin, S. A., Debey, P., Hoa, G. H. & Girault, J. P. (2004). Possible role of region 152–156 in the structural duality of a peptide fragment from sheep prion protein. *Protein Sci.* **13**, 3151–3160.
12. Kozin, S. A., Bertho, G., Mazur, A. K., Rabesona, H., Girault, J. P., Haertle, T. *et al*. (2001). Sheep prion protein synthetic peptide spanning helix 1 and beta-strand 2 (residues 142–166) shows beta-hairpin structure in solution. *J. Biol. Chem.* **276**, 46364–46370.
13. Shanmugam, G. & Jayakumar, R. (2004). Structural analysis of amyloid beta peptide fragment (25–35) in different microenvironments. *Biopolymers*, **76**, 421–434.
14. Sikorski, P., Atkins, E. D. & Serpell, L. C. (2003). Structure and texture of fibrous crystals formed by Alzheimer's abeta(11–25) peptide fragment. *Structure (Camb)*, **11**, 915–926.
15. Nelson, R., Sawaya, M. R., Balbirnie, M., Madsen, A. O., Riekel, C., Grothe, R. & Eisenberg, D. (2005). Structure of the cross-beta spine of amyloid-like fibrils. *Nature*, **435**, 773–778.
16. Nowak, M. (2004). Immunoglobulin kappa light chain and its amyloidogenic mutants: a molecular dynamics study. *Proteins: Struct. Funct. Genet.* **55**, 11–21.
17. Moraitakis, G. & Goodfellow, J. M. (2003). Simulations of human lysozyme: probing the conformations triggering amyloidosis. *Biophys. J.* **84**, 2149–2158.
18. Yang, M., Lei, M. & Huo, S. (2003). Why is Leu55→ Pro55 transthyretin variant the most amyloidogenic: insights from molecular dynamics simulations of transthyretin monomers. *Protein Sci.* **12**, 1222–1231.
19. Lei, M., Yang, M. & Huo, S. (2004). Intrinsic versus mutation dependent instability/flexibility: a comparative analysis of the structure and dynamics of wild-type transthyretin and its pathogenic variants. *J. Struct. Biol.* **148**, 153–168.
20. Ding, F., Borreguero, J. M., Buldyrey, S. V., Stanley, H. E. & Dokholyan, N. V. (2003). Mechanism for the alpha-helix to beta-hairpin transition. *Proteins: Struct. Funct. Genet.* **53**, 220–228.
21. Ikeda, K. & Higo, J. (2003). Free-energy landscape of a chameleon sequence in explicit water and its inherent alpha/beta bifacial property. *Protein Sci.* **12**, 2542–2548.
22. Daidone, I., Simona, F., Roccatano, D., Broglia, R. A., Tiana, G., Colombo, G. & Di Nola, A. (2004). Beta-hairpin conformation of fibrillogenic peptides: structure and alpha-beta transition mechanism revealed by molecular dynamics simulations. *Proteins: Struct. Funct. Genet.* **57**, 198–204.
23. Levy, Y., Hanan, E., Solomon, B. & Becker, O. M. (2001). Helix-coil transition of PrP106-126: molecular dynamic study. *Proteins: Struct. Funct. Genet.* **45**, 382–396.
24. DeMarco, M. L. & Daggett, V. (2004). From conversion to aggregation: protofibril formation of the prion protein. *Proc. Natl Acad. Sci. USA*, **101**, 2293–2298.
25. Wei, G., Mousseau, N. & Derreumaux, P. (2004). Sampling the self-assembly pathways of KFFE hexamers. *Biophys. J.* **87**, 3648–3656.
26. Urbanc, B., Cruz, L., Ding, F., Sammond, D., Khare, S., Buldyrev, S. V. *et al*. (2004). Molecular dynamics simulation of amyloid beta dimer formation. *Biophys. J.* **87**, 2310–2321.
27. Ding, F., Dokholyan, N. V., Buldyrev, S. V., Stanley, H. E. & Shakhnovich, E. I. (2002). Molecular dynamics simulation of the SH3 domain aggregation suggests a generic amyloidogenesis mechanism. *J. Mol. Biol.* **324**, 851–857.
28. Peng, S., Ding, F., Urbanc, B., Buldyrev, S. V., Cruz, L., Stanley, H. E. & Dokholyan, N. V. (2004). Discrete molecular dynamics simulations of peptide aggregation. *Phys. Rev. E*, **69**, 041908.
29. Nguyen, H. D. & Hall, C. K. (2004). Molecular dynamics simulations of spontaneous fibril formation by random-coil peptides. *Proc. Natl Acad. Sci. USA*, **101**, 16180–16185.
30. Nguyen, H. D. & Hall, C. K. (2005). Kinetics of fibril formation by polyalanine peptides. *J. Biol. Chem.* **280**, 9074–9082.
31. Gsponer, J., Haberthur, U. & Caflisch, A. (2003). The role of side-chain interactions in the early steps of aggregation: molecular dynamics simulations of an amyloid-forming peptide from the yeast prion Sup35. *Proc. Natl Acad. Sci. USA*, **100**, 5154–5159.
32. Lipfert, J., Franklin, J., Wu, F. & Doniach, S. (2005). Protein misfolding and amyloid formation for the peptide GNNQQNY from yeast prion protein Sup35: simulation by reaction path annealing. *J. Mol. Biol.* **349**, 648–658.
33. Paci, E., Gsponer, J., Salvatella, X. & Vendruscolo, M. (2004). Molecular dynamics studies of the process of amyloid aggregation of peptide fragments of transthyretin. *J. Mol. Biol.* **340**, 555–569.
34. Hwang, W., Zhang, S., Kamm, R. D. & Karplus, M. (2004). Kinetic control of dimer structure formation in amyloid fibrillogenesis. *Proc. Natl Acad. Sci. USA*, **101**, 12916–12921.

35. Klimov, D. K. & Thirumalai, D. (2003). Dissecting the assembly of Abeta16-22 amyloid peptides into antiparallel beta sheets. *Structure (Camb)*, **11**, 295–307.
36. Tsai, H. H., Reches, M., Tsai, C. J., Gunasekaran, K., Gazit, E. & Nussinov, R. (2005). Energy landscape of amyloidogenic peptide oligomerization by parallel-tempering molecular dynamics simulation: significant role of Asn ladder. *Proc. Natl Acad. Sci. USA*, **102**, 8174–8179.
37. Zanuy, D., Ma, B. & Nussinov, R. (2003). Short peptide amyloid organization: stabilities and conformations of the islet amyloid peptide NFGAIL. *Biophys. J.* **84**, 1884–1894.
38. Colombo, G., Daidone, I., Gazit, E., Amadei, A. & Di Nola, A. (2005). Molecular dynamics simulation of the aggregation of the core-recognition motif of the islet amyloid polypeptide in explicit water. *Proteins: Struct. Funct. Genet.* **59**, 519–527.
39. Wu, C., Lei, H. & Duan, Y. (2004). Formation of partially ordered oligomers of amyloidogenic hexapeptide (NFGAIL) in aqueous solution observed in molecular dynamics simulations. *Biophys. J.* **87**, 3000–3009.
40. Wu, C., Lei, H. & Duan, Y. (2005). The role of Phe in the formation of well-ordered oligomers of amyloidogenic hexapeptide (NFGAIL) observed in molecular dynamics simulations with explicit solvent. *Biophys. J.* **88**, 2897–2906.
41. Wu, C., Lei, H. & Duan, Y. (2005). Elongation of ordered peptide aggregate of an amyloidogenic peptide observed in molecular dynamics simulations with explicit solvent. *J. Am. Chem. Soc.* **127**, 13530–13537.
42. Connors, L. H., Shirahama, T., Skinner, M., Fenves, A. & Cohen, A. S. (1985). *In vitro* formation of amyloid fibrils from intact beta 2-microglobulin. *Biochem. Biophys. Res. Commun.* **131**, 1063–1068.
43. Bellotti, V., Stoppini, M., Mangione, P., Sunde, M., Robinson, C., Asti, L. *et al*. (1998). Beta2-microglobulin can be refolded into a native state from *ex vivo* amyloid fibrils. *Eur. J. Biochem.* **258**, 61–67.
44. Gejyo, F. (2000). Beta 2-microglobulin amyloid. *Amyloid*, **7**, 17–18.
45. McParland, V. J., Kalverda, A. P., Homans, S. W. & Radford, S. E. (2002). Structural properties of an amyloid precursor of beta(2)-microglobulin. *Nature Struct. Biol.* **9**, 326–331.
46. Smith, D. P., Jones, S., Serpell, L. C., Sunde, M. & Radford, S. E. (2003). A systematic investigation into the effect of protein destabilisation on beta 2-microglobulin amyloid formation. *J. Mol. Biol.* **330**, 943–954.
47. Eakin, C. M., Attenello, F. J., Morgan, C. J. & Miranker, A. D. (2004). Oligomeric assembly of native-like precursors precedes amyloid formation by beta-2 microglobulin. *Biochemistry*, **43**, 7808–7815.
48. Raman, B., Chatani, E., Kihara, M., Ban, T., Sakai, M., Hasegawa, K. *et al*. (2005). Critical balance of electrostatic and hydrophobic interactions is required for beta 2-microglobulin amyloid fibril growth and stability. *Biochemistry*, **44**, 1288–1299.
49. Ivanova, M. I., Sawaya, M. R., Gingery, M., Attinger, A. & Eisenberg, D. (2004). An amyloid-forming segment of beta2-microglobulin suggests a molecular model for the fibril. *Proc. Natl Acad. Sci. USA*, **101**, 10584–10589.
50. Kollman, P. A., Massova, I., Reyes, C., Kuhn, B., Huo, S., Chong, L. *et al*. (2000). Calculating structures and free energies of complex molecules: combining molecular mechanics and continuum models. *Accts Chem. Res.* **33**, 889–897.
51. Creighton, T. E. (1992). *Proteins: Structures and Molecular Properties*, 2nd edit., W.H. Freeman and Company, New York.
52. Thompson, J. B., Hansma, H. G., Hansma, P. K. & Plaxco, K. W. (2002). The backbone conformational entropy of protein folding: experimental measures from atomic force microscopy. *J. Mol. Biol.* **322**, 645–652.
53. Doig, A. J. & Sternberg, M. J. (1995). Side-chain conformational entropy in protein folding. *Protein Sci.* **4**, 2247–2251.
54. Duan, Y., Wu, C., Chowdhury, S., Lee, M. C., Xiong, G., Zhang, W. *et al*. (2003). A point-charge force field for molecular mechanics simulations of proteins based on condensed-phase quantum mechanical calculations. *J. Comput. Chem.* **24**, 1999–2012.
55. Onufriev, A., Case, D. A. & Bashford, D. (2002). Effective Born radii in the generalized Born approximation: the importance of being perfect. *J. Comput. Chem.* **23**, 1297–1304.
56. Darden, T., York, D. & Pedersen, L. (1993). Particle mesh Ewald. An N.Log(N) method for Ewald sums in large systems. *J. Chem. Phys.* **98**, 10089–10092.
57. Ryckaert, J. P., Ciccotti, G. & Berendsen, H. J. C. (1977). Numerical-ntegration of Cartesian equations of motion of a system with constraints—molecular-dynamics of N-alkanes. *J. Comput. Phys.* **23**, 327–341.
58. Lee, B. & Richards, F. M. (1971). The interpretation of protein structures: estimation of static accessibility. *J. Mol. Biol.* **55**, 379–400.

Edited by M. Levitt

(Received 23 August 2005; received in revised form 21 November 2005; accepted 29 November 2005)
Available online 15 December 2005